New Finite Elements for Stress Analysis around Crack in Axi-symmetric Structure†

Shuichi FUKUDA*, Hiroshi MIYAMOTO, Koichi KASHIMA***, Yasuhide SAKAGUCHI****, Takenori SHINDO***** and Yoshihisa KODAMA*******

Abstract

New finite elements, one 2 dimensional polar element and two 3 dimensional polar elements, are developed for the purpose of stress analysis around the crack in an axi-symmetric structure.

It is shown that the conventional constant stress and strain element brings about the loss of accuracy when applied to the crack in an axi-symmetric structure, because the nodal force vector deviates from the radial direction and that the ring element cannot be applied either because it cannot accomodate the circumferential displacement introduced by the crack owing to its original form of shape function.

Numerical examples of rotating bodies and of internally pressurized cylinders are analyzed and the high accuracy of these newly developed finite elements in evaluating stress intensity factors is confirmed.

1. Introduction

Many examples of axi-symmetric structures can be found in various industrial fields, such as nuclear pressure vessels, liquid storage tanks, and rotors. Most of these axi-symmetric structures are not only axi-symmetric in their geometries, but also axi-symmetric in their loading. Therefore, their displacements and stress distributions are also axi-symmetric. Considerable amount of research work have been conducted to develop suitable finite elements for studying such axi-symmetric deformations. For example, 'axi-symmetric element' or 'ring element'[1] was developed for that purpose.

But once a crack is formed in part of an axi-symmetric structure, the circumferential (θ direction) component of displacement is produced and the deformation is not axi-symmetric any more. Practical problems of cracked axi-symmetric structures are, for example, cracked coolant pipings of a nuclear reactor due to stress corrosion cracking or cracked nuclear pressure vessels due to clad welding.

It is quite important to evaluate the stress distribution around the crack tip and to evaluate stress intensity factor of an axi-symmetric structure in order to estimate the strength of structures in terms of fracture mechanics. In fact, in nuclear field, ASME Pressure Vessel and Boiler Code was updated in its 1972 summer addenda to incorporate fracture mechanics approach into its code and its latest Sec. XI recommends strongly the use of appropriate numerical technique, such as finite element method, to evaluate the values of stress intensity factor as accurately as possible[2].

Although the stress analysis of cracked axi-symmetric structures are thus important, not much work, at least to the authors' knowledge, have been carried out in developing suitable finite elements for that purpose. Therefore, most of the analyses of cracked axi-symmetric structures have been made using Cartesian-coordinate-constant-stress elements. But if constant stress elements are used, the direction of equivalent nodal force is affected by the manner of mesh divisioning so that if non-uniform meshing is adopted as in the case of meshing into finer elements around the crack to accurately evaluate the value of stress intensity factor, it brings about the loss of accuracy.

Therefore, this paper presents new finite elements which can deal with non-axi-symmetric deformation in an axi-symmetric structure based on polar coordinates or cylindrical coordinates. The cases of rotating bodies and internally pressurized cylinders are analyzed to confirm the validity of these newly developed finite elements.

† Received on March 31, 1977

* Research Instructor
** Professor, University of Tokyo
*** Researcher, Central Research Institute of Electric Power Industry
**** Senior Research Engineer, Kure Works, Babcock Hitachi, KK.
***** Research Engineer, Kure Works, Babcock Hitachi, KK.

2. Newly Developed Finite Elements

The following three types of finite elements are newly developed.

(i) 2 dimensional 4 node element (Fig. 1)
(ii) 3 dimensional 8 node element (Fig. 2)
(iii) 3 dimensional 6 node element (Fig. 3)

Figure 1 shows the 2 dimensional 4 node element.

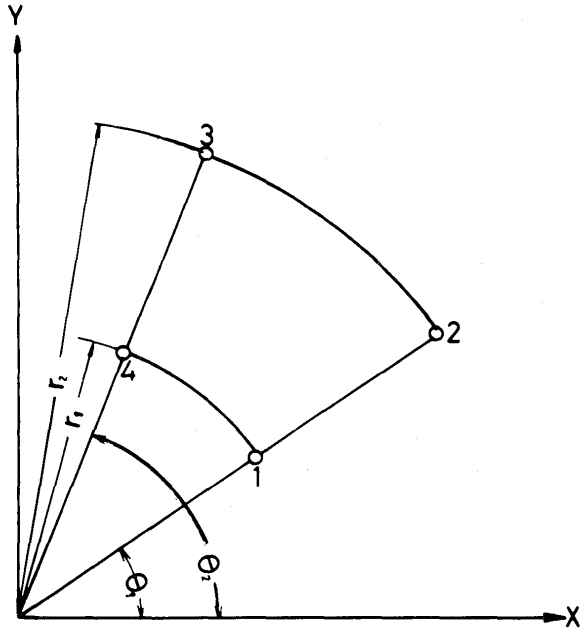

Fig. 1 2 dimensional 4 node element

The displacements in an element are expressed as follows;

$$u=a_1+a_2r+a_3\theta+a_4r\theta$$
$$v=a_5+a_6r+a_7\theta+a_8r\theta \quad (1)$$

where u and v denote the radial displacement and the circumferential displacement respectively, and $a_1 \sim a_8$ are unknown constants.

Figure 2 shows the 3 dimensional 8 node element, which is a mere extension of the above 2 dimensional 4 node element into 3 dimension. Its shape function or displacement function is given by the following form;

$$u=a_1+a_2r+a_3\theta+a_4z+a_5r\theta+a_6\theta z+a_7zr+a_8r\theta z$$
$$v=a_9+a_{10}r+a_{11}\theta+a_{12}z+a_{13}r\theta+a_{14}\theta z+a_{15}zr+a_{16}r\theta z \quad (2)$$
$$w=a_{17}+a_{18}r+a_{19}\theta+a_{20}z+a_{21}r\theta+a_{22}\theta z+a_{23}zr+a_{24}r\theta z$$

where u, v and w denote the radial, circumferential and axial displacement respectively and $a_1 \sim a_{24}$ are unknown constants.

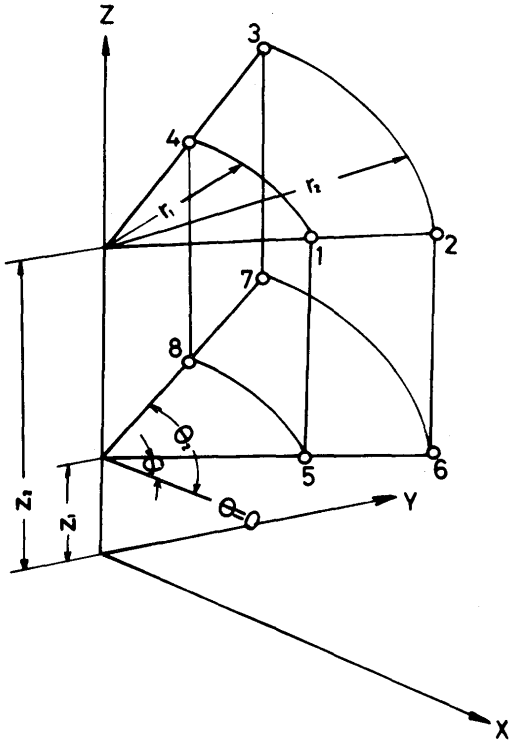

Fig. 2 3 dimensional 8 node element

Figure 3 shows the 3 dimensional 6 node element, whose cross section is triangular. Its shape function is written as,

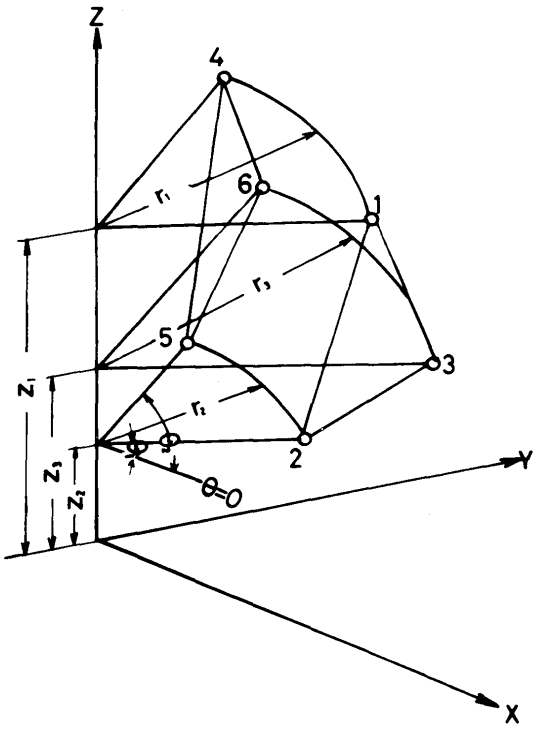

Fig. 3 3 dimensional 6 node element

$$u=(a_1+a_2r+a_3z)(a_4+a_5\theta)$$
$$v=(a_6+a_7r+a_8z)(a_9+a_{10}\theta) \quad (3)$$
$$w=(a_{11}+a_{12}r+a_{13}z)(a_{14}+a_{15}\theta)$$

where $a_1 \sim a_{15}$ are unknown constants. The 3 dimensional 6 node element has the advantage over the 8 node element in that it is much easier to represent arbitrary boundary shapes.

The reasons why these three types of newly developed finite elements are more appropriate for the analysis of cracked axi-symmetric structures than the conventional constant stress elements are;

(i) The introduction of higher order terms into the shape function brings about the improvement in accuracy.

(ii) As these elements are primarily of circular or cylindrical shape, there is no need to represent circular boundary shape by linear approximation and to divide into finer meshes in the circumferential direction to improve the accuracy of approximation as in the case of constant stress elements.

(iii) If constant stress elements are used and mesh divisioning is not uniform in the circumferential direction, the equivalent nodal force in the circumferential direction becomes non-zero and it decreases accuracy.

The point (iii) will be illustrated in the following by the case of a rotating body as an example. In the case of the 2 dimensional constant stress element, the equivalent nodal force at the node j is given by the following form;

$$F_{xj}=S\gamma\omega^2x(x_i+x_m+2x_j)/12g$$
$$F_{yj}=S\gamma\omega^2x(y_i+y_m+2y_j)/12g \quad (4)$$

where g, γ, ω, and S denote gravitation, weight of the material per unit volume, rotational angular velocity and area of the triangle respectively. When elements are divided in such a manner as shown in **Fig. 4-(1)**, the equivalent nodal forces at the node j can be expressed by the following form, since the node j is related to elements A and B.

$$\frac{F_{yj}}{F_{xj}}=\frac{S_A(y_i+y_m+2y_j)+S_B(y_m+y_k+2y_j)}{S_A(x_i+x_m+2x_j)+S_B(x_m+x_k+2x_j)} \quad (5)$$

where S_A and S_B denote the area of element A and B respectively. The equivalent nodal force turns to the radial direction only if $S_A=S_B$ holds, since the relation $F_{yj}/F_{xj}=\tan\theta_0$ holds only when $S_A=S_B$, i.e., $\theta_1=\theta_2$ and the equivalent nodal force turns to the radial direction only when this condition is satisfied as can be seen from Fig. 4-(1). This implies that elements must be divided uniformly in the circum-, ferential direction in such a manner as shown in Fig. 4-(2). And if nonuniform meshing is made as is often the case at the crack tip, non-zero component of the nodal force in the circumferential direction is produced as can be seen in Fig. 4-(3). It is apparent on the other hand that in the case of polar-coordinate elements or cylindrical-coordinate elements the direction of the nodal force is not affected by the manner of meshing in the circumferential direction as shown in Fig. 4-(4).

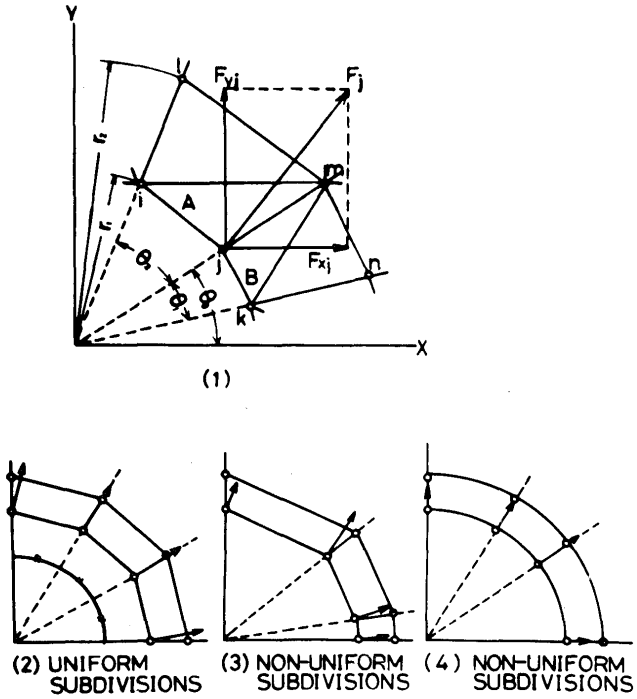

Fig. 4 Change of equivalent nodal force by meshing

A rotating disk is analyzed in the following as a numerical illustration; i.e., a rotating disk of inner radius $R_1=50$ mm, outer radius $R_2=100$ mm, rotational frequency $N=1000$ rpm, Young's modulus $E=21000$ kg/mm^2, Poisson's ratio $\nu=0.3$ and weight per unit volume $\gamma=7.86\times10^{-6}$ kg/mm^3 was analyzed using 3 dimensional composite elements composed of constant stress hexahedron elements and 3 dimensional 8 node elements. In the case of constant stress composite elements, four manners of meshing, three uniform meshing and one non-uniform meshing, are used in the calculation as in **Fig. 5**. **Figure 6** shows the comparison of the results obtained by these methods and by the following analytical solution in terms of the radial displacement u.

$$u=\frac{\gamma\omega^2r}{8Eg}\left\{(3+\nu)(1-\nu)(R_1^2+R_2^2)-(1-\nu^2)r^2+(3+\nu)(1+\nu)\frac{R_1^2R_2^2}{r^2}\right\} \quad (6)$$

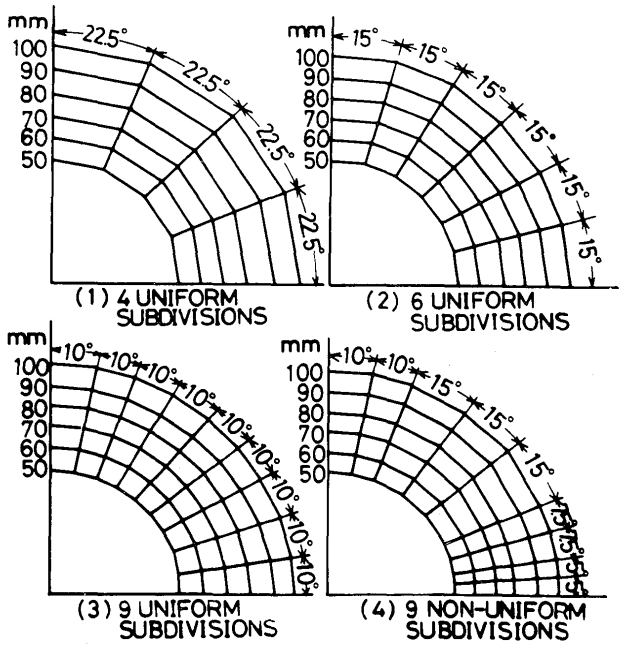

Fig. 5 Element subdivisions (constant stress element)

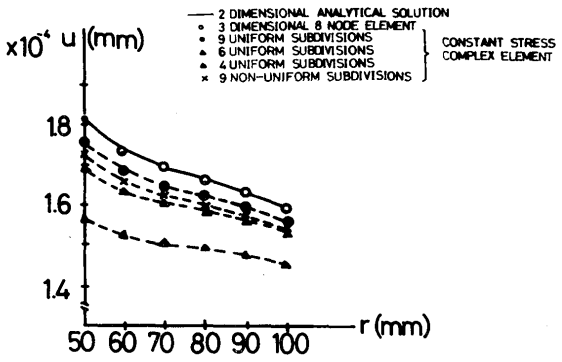

Fig. 6 Comparison of the distribution of displacement obtained by different methods

It can be observed from Fig. 6 that in the case of constant stress elements, accuracy increases and the results approach the result of the analytical solution as the number of element subdivisions increases and that accuracy decreases if meshing is not uniform. On the other hand, the result obtained using 3 dimensional 8 node elements agrees fairly well with that of the analytical solution, which fact shows the validity of the newly developed finite element.

3. Applications to Cracked Bodies

3.1 Application to Rotating Body

A hollow rotating body with two symmetric edge cracks at the inner surfaces as shown in **Fig. 7** is analyzed, using 2 dimensional 4 node elements. From symmetry, a quarter part is divided into 868 elements

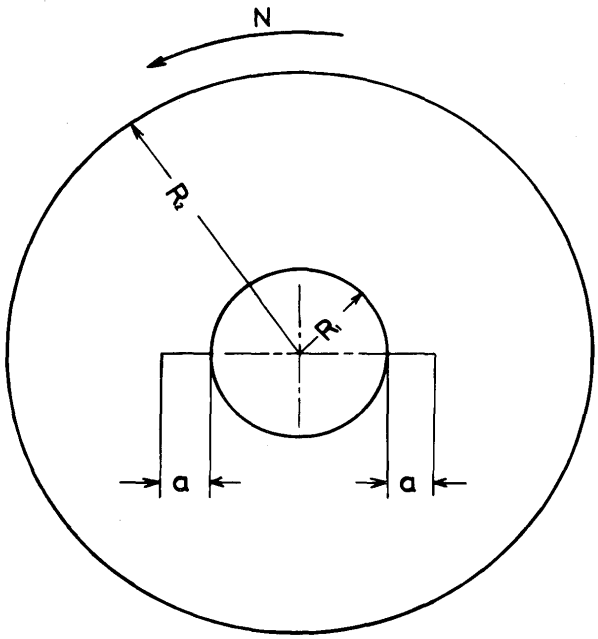

Fig. 7 Rotating Disk with two symmetric edge cracks

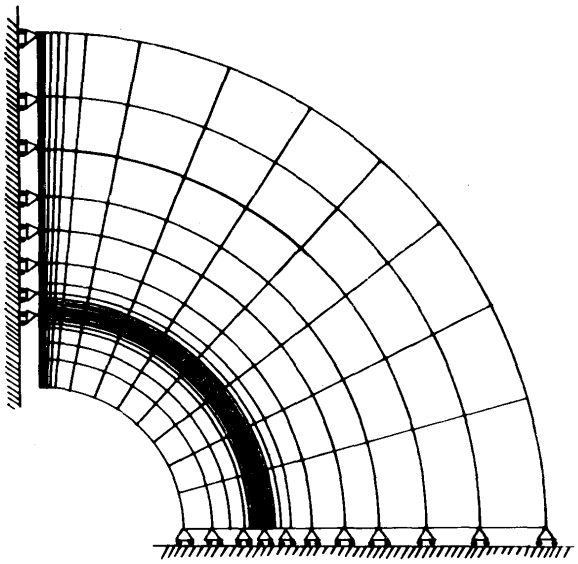

Fig. 8 Element subdivision (2 dimensional 4 node element)

and 495 nodes. The stress intensity factor K_I was calculated by three methods; (1) by averaging the K_I value obtained from the stress of the crack tip element and the K_I value obtained from crack opening displacement, (2) by using strain energy release rate G and (3) by Body Force Method[3]. The results are shown in **Table 1** for both plane stress and plane strain conditions, where the result obtained by the method (1) is shown under 'direct method', and the result obtained by method (2) is shown under 'energy method'. The equations used in the calculations are as follows;

Table 1 Dimensionless stress intensity factors for a hollow rotating body with two symmetric edge cracks at the inner surface

$R_2/R_1=10$ $a/R_1=0.5$

Plane Stress			Plane Strain		
F.E.M		Body Force Method	F.E.M		Body Force Method
Direct Method	Energy Method		Direct Method	Energy Method	
1.089	1.111	1.106	1.091	1.111	1.106

$$f_r=K_I/\sigma_0\sqrt{\pi a} \tag{7}$$

$$K_I=\sigma_0\sqrt{2\pi r'} \tag{8}$$

$$K_I=\begin{cases}\dfrac{Ev}{2(1-\nu^2)}\sqrt{\dfrac{\pi}{2r'}} & \text{(plane strain)}\\[2ex] \dfrac{Ev}{2}\sqrt{\dfrac{\pi}{2r'}} & \text{(plane stress)}\end{cases} \tag{9}$$

$$K_I=\begin{cases}\sqrt{\dfrac{GE}{1-\nu^2}} & \text{(plane strain)}\\[2ex] \sqrt{GE} & \text{(plane stress)}\end{cases} \tag{10}$$

where f_r is the stress intensity factor in dimensionless form and a, v, and r' denote crack length, crack opening displacement, and distance from the crack tip in the radial direction respectively and σ_0 means the stress at the point corresponding to the crack tip in a hollow rotating body without a crack.

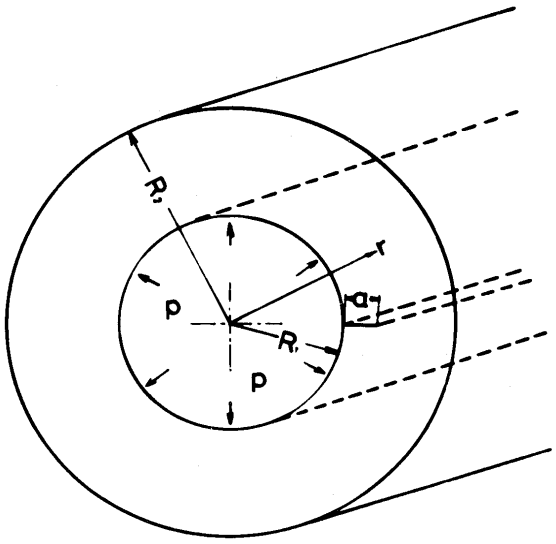

Fig. 9 Internally pressurized cylinder with a crack

3.2 Applications to Internally Pressurized Cylinders

3.2.1 2 Dimensional Analysis of Cylinder with Edge Crack

A cylinder with an edge crack of length a at the inner surface as shown in **Fig. 9** is analyzed using 2 dimensional 4 node elements. Its inner radius $R_1=50$ mm, outer radius $R_2=100$ mm, $a=15$ mm, $E=21000$ kg/mm^2, $\nu=0.3$, and internal pressure $p=10$ kg/mm^2 and the cylinder is divided into 1488 elements and 1575 nodes. Three loading conditions are analyzed in order to study the effect of internal pressure on the crack surfaces:

(i) internal pressure is applied both on the inner surface and on the crack surfaces

(ii) internal pressure is applied only on the inner surface

(iii) internal pressure is applied only on the crack surfaces

Fig. 10-(1) shows the distributions of σ_r and σ_θ on $\theta=0°$ under the condition of (i) and **Fig. 10-(2)** shows each σ_θ distribution for conditions (i), (ii) and (iii). The value of stress intensity factor is calculated using 'energy method' and its f_p value which is a

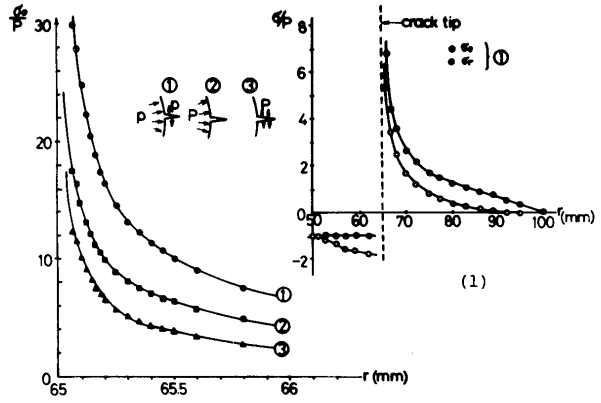

Fig. 10 Stress distributions

dimensionless stress intensity factor defined by the following equation is obtained as $f_p=2.725$.

$$f_p=K_I/p\sqrt{\pi a} \qquad (11)$$

Bowie and Freese[4] obtained the stress intensity factor for an edge-cracked hollow cylinder with its internal pressure working both on inner surface and on crack surfaces, using collocation method. As their f_p value is 2.867, both results agree fairly well.

3.2.2 3 Dimensional Analysis of Cylinder with Semi-elliptical Crack

A cylinder with a semi-elliptical crack as shown in **Fig. 11** is analyzed using 3 dimensional 6 node elements. **Figure 12** shows finite element idealization and the number of elements and nodes are 2421 and 1630 respectively. The same values as those of the preceding 2 dimensional analysis were used for R_1, R_2, a, E and ν, and a/c is chosen as parameter where $2c$ is the crack length. The analysis was made under only one loading condition that internal pressure is applied both on inner surface and on crack surfaces. **Figure 13** shows σ_θ distribution with a/c as parameter. **Figure 14** shows the distribution of crack opening displacement v. In these figures, the case that $a/c=0$ corresponds to the case of the edge crack where $c\to\infty$, and the results of $a/c=0$ are obtained using the pre-

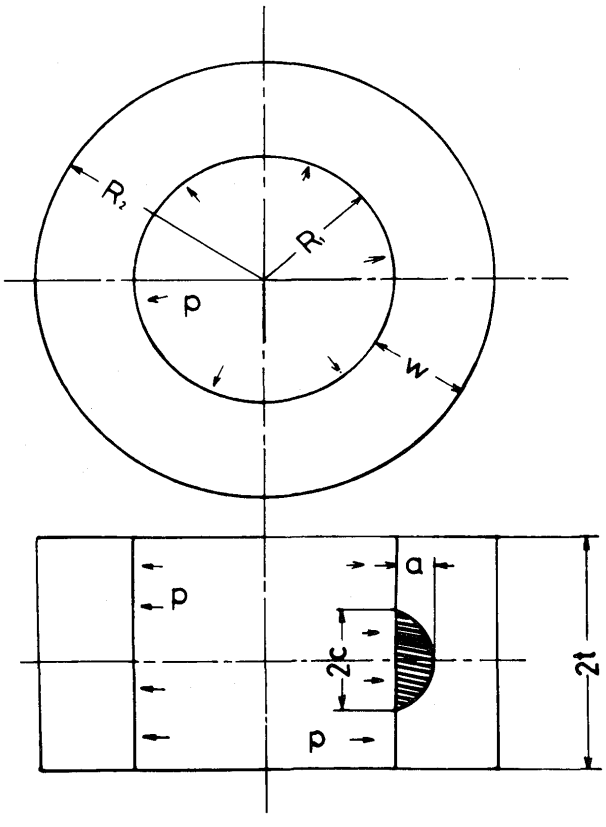

Fig. 11 Internally pressurized cylinder with a semi-elliptical crack

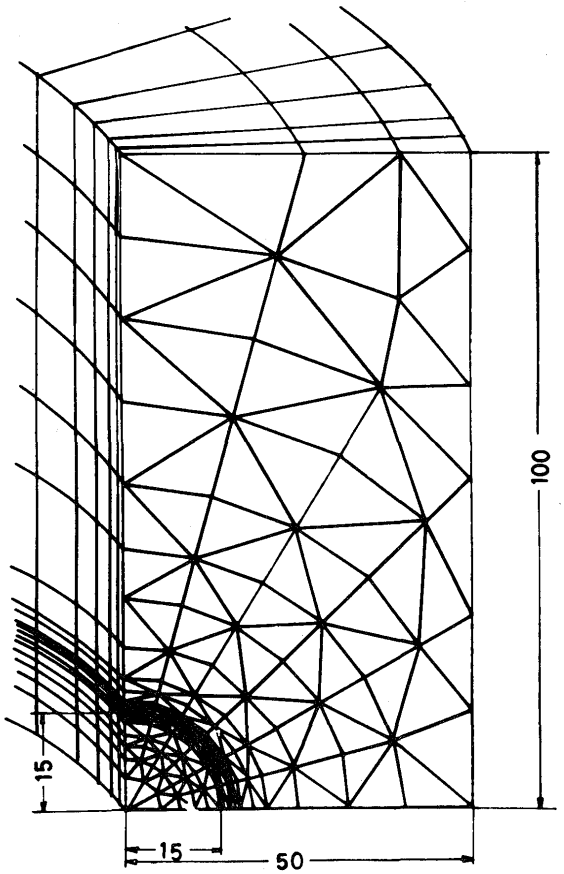

Fig. 12 Element subdivisions (3 dimensional 6 node element)

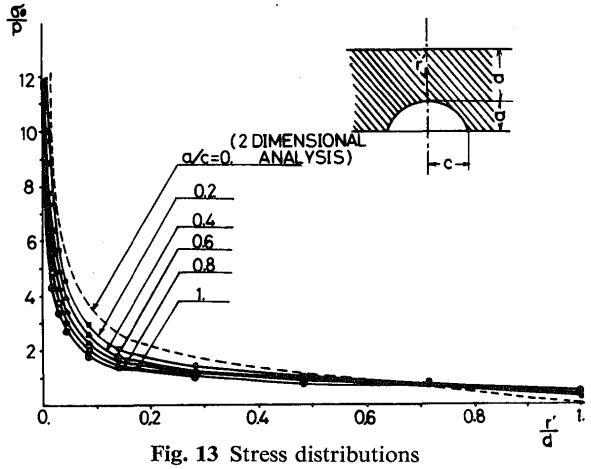

Fig. 13 Stress distributions

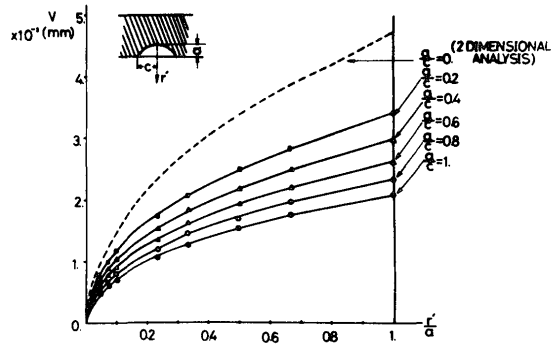

Fig. 14 Displacement distributions

ceding 2 dimensional analyses.

Table 2 shows the stress intensity factors for the internally pressurized cylinder obtained by various methods. The dimensionless stress intensity factor f_p is obtained from the crack opening displacement and the stress at the deepest crack point, using Eq. (8) and Eq. (9) and by averaging these values under the assumption of plane strain.

The dimensionless stress intensity factor f_p' is obtained in the following manner, assuming the relation[5]

$$(K_{I,se})_c=(K_{I,se})_p\,(K_{I,e})_c/(K_{I,e})_p \qquad (12)$$

where $(K_{I,se})_c=K_I$ of an internally pressurized cylinder with a semi-elliptical crack

$(K_{I,e})_c=K_I$ of an internally pressurized cylinder with an edge crack

$(K_{I,se})_p=K_I$ of a semi-infinite plate with a semi-elliptical crack

$(K_{I,e})_p=K_I$ of a semi-infinite plate with an edge crack

Here, the following formulae[6] are used for $(K_{I,e})_c$, $(K_{I,se})_p$ and $(K_{I,e})_p$.

$$(K_{I,e})_c=2.867\,p\sqrt{\pi a}\ \text{(Bowie-Freese solution)}$$

$$(K_{I,se})_p=M_1\frac{\sigma\sqrt{\pi a}}{\Phi}$$

$$(K_{I,e})_p=1.12\,\sigma\sqrt{\pi a}$$

$$M_1=1+0.12\left(1-\frac{a}{2c}\right)^2$$

$$\Phi=\int_0^{\frac{\pi}{2}}\sqrt{\frac{a^2}{c^2}\cos^2\theta+\sin^2\theta}\;d\theta$$

where M_1 is the correction factor for front surface[7] and σ is the uniform tensile stress and Φ is the complete elliptical integral of the second kind.

Therefore, $(K_{I,se})_c$ can be obtained as follows;

$$(K_{I,se})_c=2.867\frac{M_1}{1.12\Phi}p\sqrt{\pi a}$$

The dimensionless stress intensity factor f_p' is

$$f_p'=2.867\frac{1+0.12\left(1-\frac{a}{2c}\right)^2}{1.12}$$

The dimensionless stress intensity factor f_p'' is obtained in the following manner. The stress intensity factor for an edge crack in a semi-infinite plate which is subjected to the stress and internal pressure p is given by,

$$K_I=1.12\sigma_1\sqrt{\pi a}+1.12p\sqrt{\pi a}$$

where σ_1 is the circumferential stress at the point corresponding to 'crack tip' of an internally pressurized cylinder without a crack. If we write $W=R_2/R_1$, $\lambda=a/R_1$, $W=R_2-R_1$, σ_1 is given by

$$\sigma_1=\frac{pR_1^2}{R_2^2-R_1^2}\left\{\frac{R_2^2}{(R_1+a)^2}+1\right\}$$

$$=\frac{p}{W^2-1}\left\{\frac{W^2}{(1+\lambda)^2}+1\right\}$$

therefore, $K_I=1.12\,p\sqrt{\pi a}\left\{\frac{W^2/(1+\lambda)^2+1}{W^2-1}+1\right\}$

The above equation is extended to a semi-elliptical crack by introducing the correction factor M_1 for front surface, the correction factor M_2 for back surface[6] and Φ.[8]

$$K_I=M_1M_2\frac{p\sqrt{\pi a}}{\Phi}\left\{\frac{W^2/(1+\lambda)^2+1}{W^2-1}+1\right\}$$

Table 2 Dimensionless stress intensity factors for an internally pressurized cylinder with a semi-elliptical crack at the inner surface

$R_2/R_1=2$ $\quad a/R_1=0.3$

a/c	0	0.2	0.4	0.6	0.8	1.0
F.E.M (f_p)	2.725	2.358	2.055	1.797	1.578	1.394
Bowie-Freese	2.867					
f_p'	2.867	2.674	2.396	2.123	1.883	1.679
f_p''	2.472	2.305	2.065	1.831	1.623	1.447

where $M_2=\sqrt{\frac{2W}{\pi a}\tan\frac{\pi a}{2W}}$

Therefore, the dimensionless stress intensity factor f_p'' is obtained as follows;

$$f_p''=\frac{M_1M_2}{\Phi}\left\{\frac{W^2/(1+\lambda)^2+1}{W^2-1}+1\right\}$$

It is observed from Table 2 that f_p can be approximated by f_p'' except when a/c is close to zero.

4. Summary

New finite elements which can analyze non-axi-symmetric deformation due to crack in an axi-symmetric structure are developed. These newly developed polar-coordinate or cylindrical-coordinate elements can provide more accurate solutions because these elements do not produce the error of the equivalent nodal force in the circumferential direction, even if meshing is non-uniform in the circumferential direction.

These newly developed finite elements are, therefore, believed to be quite useful for fracture mechanics analysis.

References

1) O. C. Zienkiewicz and Y. K. Cheung, "The Finite Element Method in Structural and Continuum Mechanics" McGraw-Hill Publishing Company.
2) S. Fukuda, "Preliminary Survey on the Reliability of the Fast Breeder Reactor Piping System", pp. 18–31. Nuclear Safety Research Association (in Japanese)
3) Y. Murakami and H. Nisitani, "The Stress Intensity Factors for the Cracked Hollow Spin Disk" Proc. JSME, Vol. 41, No. 348, p. 2255.
4) O. L. Bowie and C. E. Freese, Eng. Frac. Mech. Vol. 4, No. 2 1972, p. 315.
5) J. H. Anderwood, ASTM STP 513, 1972, p. 59.
6) P. C. Paris and G. C. Sih, ASTM STP 381, 1965, p. 30.
7) A. S. Kobayashi and W. L. Moss, Fracture, p. 31, Chapman and Hall Ltd.
8) Kunio Nishioka, Kenji Hirakawa and Ikushi Kitaura, "Fatigue Strength of Thick-walled Cylinders under Cyclic Internal Pressure (Fatigue Crack Growth and the Effect of Internal Flaw)", Journal of High Pressure Institute, Vol. 12, No. 3, 1974, pp. 16–22. (in Japanese)